

Charmed meson masses and decay constants in the continuum from the tadpole improved clover ensembles (CLQCD Collaboration)



Hai-Yang Du,^{1,2} Bolun Hu,² Ying Chen,^{1,3} Heng-Tong Ding,⁴ Chuan Liu,^{5,6,7} Liuming Liu,^{8,9}
Yu Meng,¹⁰ Peng Sun,^{8,*} Ji-Hao Wang,^{1,2} Yi-Bo Yang,^{1,2,11,12,†} and Dian-Jun Zhao^{1,2}

¹University of Chinese Academy of Sciences, School of Physical Sciences, Beijing 100049, China

²CAS Key Laboratory of Theoretical Physics, Institute of Theoretical Physics,
Chinese Academy of Sciences, Beijing 100190, China

³Institute of High Energy Physics, Chinese Academy of Sciences, Beijing 100049, China

⁴Key Laboratory of Quark & Lepton Physics (MOE) and Institute of Particle Physics,
Central China Normal University, Wuhan 430079, China

⁵School of Physics, Peking University, Beijing 100871, China

⁶Center for High Energy Physics, Peking University, Beijing 100871, China

⁷Collaborative Innovation Center of Quantum Matter, Beijing 100871, China

⁸Institute of Modern Physics, Chinese Academy of Sciences, Lanzhou, 730000, China

⁹University of Chinese Academy of Sciences, Beijing 100049, China.

¹⁰School of Physics, Zhengzhou University, Zhengzhou, Henan 450001, China

¹¹School of Fundamental Physics and Mathematical Sciences,
Hangzhou Institute for Advanced Study, UCAS, Hangzhou 310024, China

¹²International Centre for Theoretical Physics Asia-Pacific, Beijing/Hangzhou, China

(Dated: August 8, 2024)

We present the determination of the charm quark mass, the masses and decay constants of charmed mesons using thirteen 2+1 flavor full-QCD gauge ensembles at five different lattice spacings $a \in [0.05, 0.11]$ fm, 8 pion masses $m_\pi \in (130, 360)$ MeV, and several values of the strange quark mass, which facilitate us to do the chiral and continuum extrapolation. These ensembles are generated through the stout smeared clover fermion action and Symanzik gauge actions with the tadpole improvement. Using QED-subtracted D_s meson mass and non-perturbative renormalization, we predict the charm quark mass in the continuum with physical light and strange quark masses to be $m_c(m_c) = 1.289(17)$ GeV in $\overline{\text{MS}}$ scheme, with the systematic uncertainties from lattice spacing determination, renormalization constant, and fit ansatz included. Predictions of the open and close charm mesons using this charm quark mass agree with the experimental value at 0.3% level uncertainty. We obtained $D_{(s)}$ decay constants and also by far the most precise $D_{(s)}^*$ decay constants $f_{D^*} = 0.2321(43)$ GeV and $f_{D_s^*} = 0.2743(34)$ GeV, with the charm quark improved vector current normalization.

I. INTRODUCTION

Lattice QCD has proven to be highly effective in providing first-principle predictions for the non-perturbative characteristics of light quarks with $m_q \ll \Lambda_{\text{QCD}}$. On the other hand, the lattice QCD prediction of the hadron spectrum and structure involving heavy quarks with $m_Q \gg \Lambda_{\text{QCD}}$ is also highly demanded. This is necessary for constraining the CKM matrix elements through the weak decay constant of hadrons, as well as for determining Higgs coupling to heavy quarks. Furthermore, lattice

QCD calculations are crucial for revealing the nature of extraordinary hadron states such as tetraquarks [1, 2] and pentaquarks [3, 4].

However, the lattice QCD calculations for heavy quarks with $m_Q \gg \Lambda_{\text{QCD}}$ are significantly more challenging. The primary difficulty arises from the fact that the heavy quark mass can introduce additional discretization errors of the order $m_Q^2 a^2$, and even the $m_Q^4 a^4$ corrections can become significant when $a \sim 0.1$ fm and $m_Q \sim 1$ GeV. Thus comparing to the light flavor case, the calculations at more lattice spacings are very beneficial to control the systematic uncertainty from the discretization error.

In this work, we use the 2+1 flavor full-QCD ensembles generated by the CLQCD collaborations at 5 lat-

* Corresponding author: pengsun@impcas.ac.cn

† Corresponding author: ybyang@itp.ac.cn

tice spacings to determine the charm quark mass and charmed meson properties. As discussed in the recent lattice average of flavor physics [5], the systematic uncertainty stemming from the absence of the charm quark as a dynamical degree of freedom in the action is expected to be at a level of a few percent. This is due to the decoupling of the heavy quark with $m_Q \gg \Lambda_{\text{QCD}}$, and will be revisited once dynamical charm ensembles become available. Additionally, the QED effects of the charm quark mass are considered based on calculations from the literature [6], although they are not included in our predictions of hadron masses and decay constants. We expect that this systematic uncertainty will be under control in the near future, using the infinite volume reconstruction techniques [7].

Comparing to the previous charm quark mass determination using the clover fermion action [8], our calculation applies the stout smearing on the gauge field used by the fermion action, thereby offering a validation of the systematic uncertainty associated with the fermion action definition. We also investigate the sensitivity of meson decay constants to the discretization of the normalization constant Z_V , noting that this sensitivity is eliminated by the fact that the renormalization of the PCAC quark mass only requires the ratio Z_A/Z_P of the renormalization constants.

The organization of this work is outlined as follows. Section II presents the numerical setup, which includes the interpolation of strange and charm quark masses, the definition of different normalization constants, and their lattice spacing dependence. Section III shows the continuum extrapolation of the renormalized charm mass and hadron properties, and also comparison with the experiment and previous calculations. Finally, Section IV offers a concise summary and discussion.

II. NUMERICAL SETUP

The results in this work, are based on the 2+1 flavor full QCD ensembles from the CLQCD collaboration using the tadpole improved tree level Symanzik (TITLS) gauge action and the tadpole improved tree level Clover (TITLC) fermion action. In addition to the ensembles employed for determining the light quark masses and low energy constants [9], we have included two additional ensembles, E28P35 and G36P29, with $m_\pi \sim 300$ MeV and gauge couplings $\hat{\beta} = 6.308$ and 6.498 to manage discretization errors. By using these two values of $\hat{\beta}$, self consistent u_0 and v_0 , and also the lattice spacing determined through the gradient flow [10] with w_0 [11] using the Symanzik action, the spatial volume of the E28P35 and G36P29 ensembles are similar to those of the other ensembles with $m_\pi \sim 300$ MeV. The parameters employed for the simulation are outlined in Table I, and we use \hat{O} for the dimensionless value of any quantity O .

The variance of binned means of the plaquette $\square = \langle \text{Tr } U_p \rangle / 3$, topological charge Q , pion mass m_π , and η_c

mass m_{η_c} as shown in the appendix, suggest that the autocorrelation between configurations is acceptable. This is particularly evident in the case of Q , which does not exhibit any indications of topological charge freezing at the smallest lattice spacing $a = 0.0519(3)$ fm.

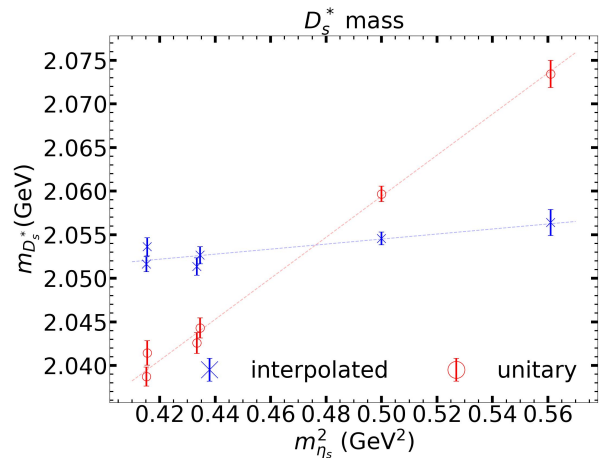


FIG. 1. The $m_{\eta_s}^2$ dependence of the D_s^* mass at $a = 0.1053$ fm, with unitary strange quark mass parameter (red dots) and interpolated one (blue crosses).

Given that the unitary strange quark mass on some ensembles deviate by 10-15% from the physical strange quark mass, we have adjusted the interpolated valence strange quark mass \tilde{m}_s^I to that correspond to the “physical” η_s mass of $689.89(49)$ MeV [12] on each ensemble to mitigate this discrepancy. This η_s mass aligns with our previous determination $m_{\eta_s} = 687.4(2.2)$ MeV on CLQCD ensembles but with significantly reduced uncertainties. Fig. 1 illustrates the strange quark mass dependence (through $m_{\eta_s}^2$) of the D_s^* meson mass at $a = 0.1053$ fm and interpolated charm quark mass, using either the unitary strange quark mass parameter \tilde{m}_s (red circles) or the interpolated parameter \tilde{m}_s^I (blue crosses). The strange quark mass dependence of the latter case is only 10% of the former case and then allows a more reliable continuum extrapolation since the contribution of the cross term like $m_{\eta_s}^2 a^2$ will be highly suppressed. This residual mismatch effect of the sea strange quark mass will be addressed through a joint fit using all the ensembles.

Determining the valence charm quark mass can present additional complexities. The physical J/ψ or η_c mass should account for both the disconnected charm quark contribution and QED effect, making it unsuitable for accurately determining the charm quark mass using pure QCD calculations with only the connected charm quark contribution. Conversely, the open-charm pseudoscalar meson masses is free of the disconnected valence charm quark contribution, and its QED effect has been computed in previous literature [6] and updated in Ref. [13]. Compared to the strange quark, the valence light quark

TABLE I. Gauge coupling $\hat{\beta} = 10/(g^2 u_0^4)$, lattice spacing a , tadpole improvement factors u_0 and v_0 , dimensionless bare quark mass parameters $\tilde{m}_{l,s}^b$, Lattice size $\tilde{L}^3 \times \tilde{T}$, corresponding pion mass m_π and η_s mass m_{η_s} , interpolated bare strange and charm quark mass parameters $\tilde{m}_{s,c}^I$, and the statistics information.

Symbol	$\hat{\beta}$	a (fm)	u_0	v_0	\tilde{m}_l^b	\tilde{m}_s^b	$\tilde{L}^3 \times \tilde{T}$	m_π (MeV)	m_{η_s} (MeV)	\tilde{m}_s^I	\tilde{m}_c^I	$n_{\text{cfg}} \times n_{\text{src}}$
C24P34	6.200	0.10530(18)	0.855453	0.951479	-0.2770	-0.2310	$24^3 \times 64$	340.5(1.7)	748.99(73)	-0.2396(2)	0.4080(26)	200×32
C24P29			0.855453	0.951479	-0.2770	-0.2400	$24^3 \times 72$	292.7(1.2)	658.29(65)	-0.2357(2)	0.4168(26)	760×3
C32P29			0.855453	0.951479	-0.2770	-0.2400	$32^3 \times 64$	292.4(1.1)	659.22(41)	-0.2358(2)	0.4158(26)	489×3
C32P23			0.855520	0.951545	-0.2790	-0.2400	$32^3 \times 64$	228.0(1.2)	644.36(45)	-0.2338(2)	0.4198(26)	400×3
C48P23			0.855520	0.951545	-0.2790	-0.2400	$48^3 \times 96$	225.6(0.9)	644.58(62)	-0.2338(2)	0.4214(26)	62×3
C48P14			0.855548	0.951570	-0.2825	-0.2310	$48^3 \times 96$	135.5(1.6)	707.06(44)	-0.2335(2)	0.4212(26)	188×3
E28P35	6.308	0.08877(30)	0.859646	0.954385	-0.2490	-0.2170	$28^3 \times 64$	352.1(1.2)	720.31(94)	-0.2204(3)	0.2707(37)	147×4
F32P30	6.410	0.07750(18)	0.863437	0.956942	-0.2295	-0.2050	$32^3 \times 96$	303.2(1.3)	677.6(1.0)	-0.2039(2)	0.1968(21)	250×3
F48P30			0.863473	0.956984	-0.2295	-0.2050	$48^3 \times 96$	303.4(0.9)	676.32(62)	-0.2038(2)	0.1949(21)	99×3
F32P21			0.863488	0.957017	-0.2320	-0.2050	$32^3 \times 64$	210.9(2.2)	660.27(94)	-0.2024(2)	0.1989(21)	194×3
F48P21			0.863499	0.957006	-0.2320	-0.2050	$48^3 \times 96$	207.2(1.1)	663.39(65)	-0.2026(2)	0.1991(21)	82×12
G36P29	6.498	0.06826(27)	0.866476	0.958910	-0.2150	-0.1926	$36^3 \times 108$	295.1(1.2)	693.2(1.0)	-0.1929(2)	0.1378(28)	68×4
H48P32	6.720	0.05187(26)	0.873378	0.963137	-0.1850	-0.1700	$48^3 \times 144$	317.2(0.9)	695.9(1.3)	-0.1703(2)	0.0533(24)	157×12

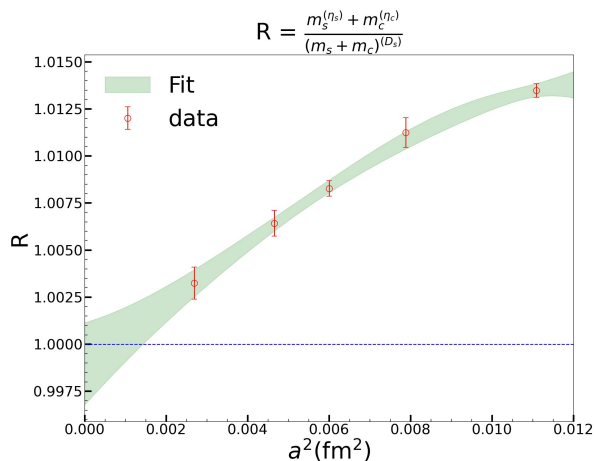


FIG. 2. The ratio of the PCAC quark mass determined from the quarkonium, and also D_s . Two definitions are consistent up to $\mathcal{O}(a^4)$ correction.

with physical mass is noisy, costly, and also susceptible to significant finite-volume effects on most of our ensembles. Thus the optimal choice to determine the interpolated valence charm quark mass parameter \tilde{m}_c^I on each ensemble, is requiring the D_s meson mass to be the QED effect subtracted physical value [13] under the GRS renormalization scheme $m_{q,\text{QCD+QED}}^{\overline{\text{MS}}}(2\text{GeV}) = m_{q,\text{QCD}}^{\overline{\text{MS}}}(2\text{GeV})$ [14],

$$m_{D_s}^{\text{QCD}} = m_{D_s}^{\text{phys}} - \Delta^{\text{QED}} m_{D_s} = 1966.7(1.5) \text{ MeV}. \quad (1)$$

The values of the interpolated strange and charm quark masses $\tilde{m}_{s,c}^I$ are also presented in Table I, based on the polynomial interpolation of the calculations of m_{η_s, D_s} using three strange (charm) mass parameters. The sensitivity of $\tilde{m}_{s,c}^I$ to the light and strange sea quark mass and lattice volume is on the order of a few MeV and should be eliminated upon extrapolation to physical quark masses and the infinite volume limit.

Similar to the previous CLQCD study on the light and strange quarks [9], we define the PCAC charm quark mass through the PCAC relation [15]:

$$m_q^{\text{PC}} = \frac{m_{\text{PS}} \sum_{\vec{x}} \langle A_4(\vec{x}, t) P^\dagger(\vec{0}, 0) \rangle}{2 \sum_{\vec{x}} \langle P(\vec{x}, t) P^\dagger(\vec{0}, 0) \rangle} \Big|_{t \rightarrow \infty}. \quad (2)$$

where $A_\mu = \bar{\psi} \gamma_5 \gamma_\mu \psi$, $P = \bar{\psi} \gamma_5 \psi$, and m_{PS} is the corresponding pseudoscalar meson mass.

In Fig. 2, we show the ratio of two determinations of $m_s + m_c$ from quarkonium (η_s and η_c) and also D_s , at five lattice spacings, with the interpolated strange and charm quark masses. Two determinations deviate from each other by approximately 1.4% at the coarsest lattice spacing but are consistent within the statistical uncertainty of 0.1% after a polynomial extrapolation up to $\mathcal{O}(a^4)$ to the continuum limit.

The renormalized quark mass can be subsequently defined as $m_q^R = Z_A / Z_P m_q^{\text{PC}}$. The ratio Z_A / Z_P can be extracted from the corresponding amputated vertex functions $\Lambda_{A,P}$ in the off-shell quark state with momentum p under the Landau gauge [9],

$$\frac{Z_A}{Z_P(\mu)} = \frac{\frac{1}{12} \text{Tr}[\Lambda_P(p) \gamma_5]}{\frac{1}{48} \text{Tr}[\Lambda_A^\mu(p) \gamma_\mu \gamma_5]} \Big|_{p^2 = \mu^2}, \quad (3)$$

subtracting the $1/m_q$ mass pole of the Goldstone meson [16] and extrapolating to the chiral limit. $\Lambda_{\mathcal{O}}(p) = S^{-1}(p) G_{\mathcal{O}}(p) S^{-1}(p)$ can be obtained from the quark propagators $S(p) = \sum_x e^{-ip \cdot x} \langle \psi(x) \bar{\psi}(0) \rangle$ and also $G_{\mathcal{O}}(p) = \sum_{x,y} e^{-ip \cdot (x-y)} \langle \psi(x) \mathcal{O}(0) \bar{\psi}(y) \rangle$.

Following the previous light quark study on the same ensembles, we use the coulomb wall source propagator to suppress the statistical uncertainty, and extract the meson mass and local operator matrix elements through the joint fit of the wall-to-point and wall-to-wall two point functions [9]. The number of the configuration n_{cfg} and sources used per configuration n_{src} are also collect in Table I. Then the meson decay constants can be extracted

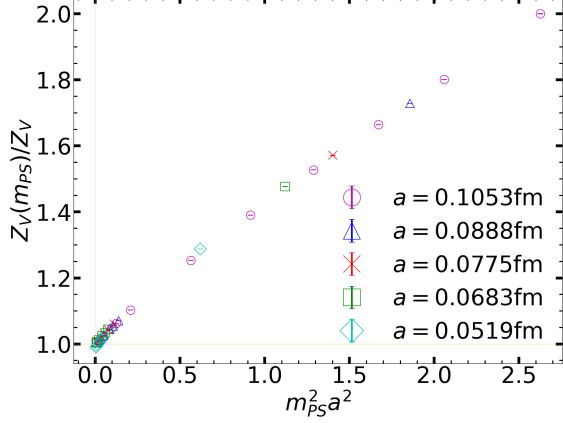


FIG. 3. The dimensionless pseudo-scalar mass $m_{\text{PS}}^2 a^2$ dependence of Z_V using the pseudo-scalar meson mass, at different lattice spacing.

from the matrix elements with proper normalization,

$$\begin{aligned} Z_V \langle 0 | V^\mu | V_i \rangle &= \epsilon_i^\mu m_V f_V, \\ Z_T \langle 0 | T^{4i} | V_j \rangle &= \delta_j^i m_V f_V^T, \\ Z_A \langle 0 | P | \text{PS} \rangle &= \frac{m_{\text{PS}}^2}{2m_q^{\text{PC}}} f_{\text{PS}}, \end{aligned} \quad (4)$$

where $V_\mu = \bar{\psi} \gamma_\mu \psi$, $T_{\mu\nu} = \bar{\psi} \gamma_\mu \gamma_\nu \psi$, $|\text{PS}\rangle$ ($|V\rangle$) is the pseudoscalar (vector) meson state, and $Z_{T,V,A}$ is the tensor, vector and axial-vector current normalization constants, respectively. Additionally, one can define the decay constants of the P-wave charmonium as

$$\begin{aligned} Z_S \langle 0 | \bar{c}c | \chi_{c0} \rangle &= m_{\chi_{c0}} f_{\chi_{c0}}, \\ Z_A \langle 0 | \bar{c} \gamma_3 \gamma_5 c | \chi_{c1} \rangle &= m_{\chi_{c1}} f_{\chi_{c1}}, \\ Z_T \langle 0 | \bar{c} \sigma_3 c | h_c \rangle &= m_{h_c} f_{h_c}, \end{aligned} \quad (5)$$

using the renormalization constants $Z_{S,A,T}$.

For the clover fermion, the ratio between Z_A and Z_V ,

$$\frac{Z_A}{Z_V} = \frac{\frac{1}{12} \text{Tr}[\Lambda_V(p) \gamma_\mu]}{\frac{1}{48} \text{Tr}[\Lambda_A^\mu(p) \gamma_\mu \gamma_5]}, \quad (6)$$

can deviate from 1 due to additive chiral symmetry breaking, and it is essential to include this effect to obtain correct $f_{\pi,K}$ after the continuum extrapolation [9]. More detailed discussion on the ratio

$$\frac{Z_T}{Z_V} = \frac{\frac{1}{12} \text{Tr}[\Lambda_V(p) \gamma_\mu]}{\frac{1}{72} \text{Tr}[\Lambda_T^{\mu\nu}(p) \gamma_\nu \gamma_\mu]}, \quad (7)$$

can be found in our previous work [9].

Therefore, all renormalization constants can be obtained by taking their ratio over Z_V , once Z_V is determined. But unlike its continuum counterpart, Z_V under

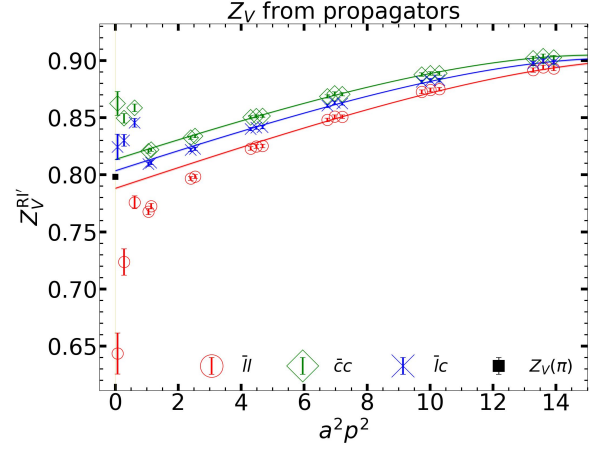


FIG. 4. $Z_V^{\text{RI}'}$ from the Landau gauge fixed propagators for the quark bilinear operators $\bar{l}l$ (red circles), $\bar{l}c$ (blue crosses), and $\bar{c}c$ (green boxes), at $a = 0.1053$ fm. After the $a^2 p^2$ extrapolation with $a^2 p^2 \geq 4$ shown as the curves, the extrapolated values agree with the chiral extrapolated value $Z_V(\pi) = 0.79814(23)$ within 2%.

lattice regularization is subject to both α_s and a^2 corrections and can be determined from the vector current conservation condition [17, 18],

$$Z_V(H) \frac{\langle H | V_4 | H \rangle}{\langle H | H \rangle} = 1, \quad (8)$$

where H represents an arbitrary hadronic state. $Z_V(H)$ should be independent of H in the continuum due to charge conservation, while it can suffer from a significant $m_q a$ error at finite lattice spacing. In Fig. 3, we show that $Z_V(\text{PS})$ is almost a single function of $m_{\text{PS}}^2 a^2$ and insensitive to lattice spacing, after it is normalized by $Z_V(\pi)$ in the chiral limit. Based on the joint fit, it can be approximated by the following relation,

$$\begin{aligned} Z_V(\text{PS}; a) &= Z_V(0) \{ 1 + (0.587(9) - 0.43(6)a^2) m_{\text{PS}}^2 a^2 \\ &\quad - (0.131(8) - 0.35(4)a^2) m_{\text{PS}}^4 a^4 + \mathcal{O}(m_{\text{PS}}^6 a^6) \}. \end{aligned} \quad (9)$$

at 0.3% level.

At the same time, one can also calculate Z_V through the quark propagators directly,

$$Z_V^{\text{RI}'}(a, a^2 p^2) = \frac{C_V Z_q}{\frac{1}{48} \text{Tr}[\Lambda_V^\mu(p) \gamma_\mu]}, \quad (10)$$

where $Z_q = \frac{-i}{12\hat{p}^2} \text{Tr}[S^{-1}(p)\hat{p}]$ with $\hat{p}_\mu = \sin(p_\mu a)/a$, and

$$C_V = \frac{\text{Tr}[\Lambda_V^\mu(p) \gamma_\mu]}{\text{Tr}[\Lambda_V^\mu(p) \gamma_\nu (g_{\mu\nu} - \frac{p_\mu p_\nu}{p^2})]} \quad (11)$$

can be calculated perturbatively to avoid the discretization error in the off-diagonal projection $\text{Tr}[\Lambda_V^\mu(p) \gamma_{\nu \neq \mu}]$. As shown in Fig. 4, it is surprising that $Z_V^{\text{RI}'}$ for the quark

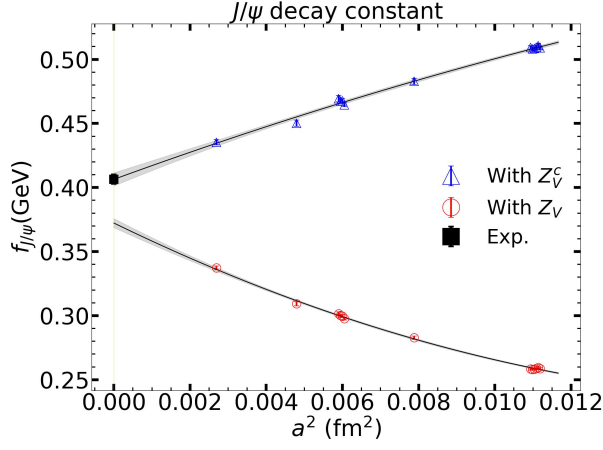


FIG. 5. Comparison of $f_{J/\psi}$ using heavy quark improved and original normalization constants Z_V , at different lattice spacing and continuum. The experimental value is also shown as black boxes for comparison.

bilinear operators $\bar{l}l$ (red circles), $\bar{l}c$ (blue crosses), and $\bar{c}c$ (green boxes) for the light quark l and charm quark c are similar within $\sim 1\%$ in the perturbative region $p^2 \geq (5\text{GeV})^2$, and their $a^2 p^2$ extrapolated values based on the values in the perturbative region are also consistent with Z_V in the chiral limit with 2%, as illustrated in Fig. 3 at the largest lattice spacing where $Z_V(\eta_c)$ for the charm quark is around 2 times of $Z_V(\pi)$. Thus, the $a^2 m_{\text{PS}}^2$ dependence of Z_V would be an additional discretization effect of the heavy quark in the hadron.

Fig. 5 displays the values of $f_{J/\psi}$ at various lattice spacings using either $Z_V^c \equiv Z_V(\eta_c)$ (blue triangles) or $Z_V \equiv Z_V(\pi)_{m_\pi \rightarrow 0}$ (red circles). It is evident that employing the heavy quark improved normalization Z_V^c leads to significantly smaller discretization errors and also better agreement with the experimental value $406.5(3.7)(0.5)$ MeV [19, 20] after the continuum extrapolation, compared to the case with the chiral extrapolated normalization Z_V .

The improvement in suppressing discretization errors for heavy flavor matrix elements can be extended to other currents as well. For instance, considering $g_{S,\text{ME}}(H) \equiv \frac{\langle H|S|H\rangle}{\langle H|H\rangle}$ as illustrated in Fig. 6, one can use the original Z_S (red circles) for the $\bar{c}c$ matrix element in the η_c , akin to the treatment for $\bar{l}l$ in the pion, or opt for the heavy quark improved $Z_S^c \equiv Z_V^c \frac{Z_S}{Z_V}$ (blue triangles) to mitigate discretization errors. Additionally, we present $g_{S,\text{FH}} \equiv \frac{\partial m_{\eta_c}}{\partial m_c^2} = \frac{Z_S}{Z_A} \frac{\partial m_{\eta_c}}{\partial m_c^2 \text{PAC}}$ (green crosses) for comparison, which should align with $g_{S,\text{ME}}$ in the continuum. Upon continuum extrapolation, all these quantities converge, while $g_{S,\text{ME}}$ renormalized by Z_S exhibits a larger discretization error.

The improvement can be extended to the flavor-changed current, like $X \equiv \bar{c}l$, by utilizing the improved renormalization constant $Z_X^c \equiv \sqrt{Z_V Z_V^c} \frac{Z_X}{Z_V}$. As shown

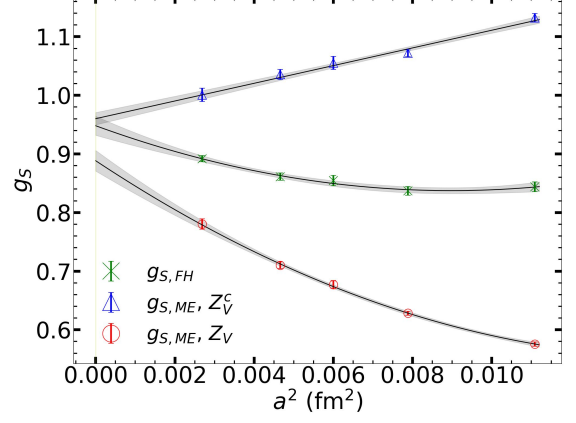


FIG. 6. Comparison of $\bar{c}c$ scalar matrix element in η_c using original and heavy quark improved normalization constants Z_V , and also that from the Feynman-Hellman theorem, at different lattice spacing and continuum.

in Fig. 7, for the decay constant of D_s^* , we can see that the use of the heavy quark improved renormalization constant can reduce the discretization error significantly, while the continuum limit from both cases agree with each other. Similar improvement could be used for decay constant of the other open-charm meson, such as f_D , as discussed in the following section.

As shown in Eq. (9), the $O(a^6 m_{\text{PS}}^2)$ term is necessary to describe the $m_{\text{PS}}^2 a^2$ dependence of $Z_V(\text{PS}; a)$. Thus the differences between the $f_{J/\psi}$ and g_{S,η_c} results using Z_V and Z_V^c are the $O(a^6)$ effect which is not included in the current fit ansatz, especially the cases using the chiral extrapolated Z_V in the charmonium matrix elements. Since using Z_V^c can significantly suppress the discretization error, we will only use Z_V^c for all the following discussion when the charm quark is involved.

At the end of this section, we apply the joint fit of the renormalization constants using the following form to obtain the values at the chiral limit of the sea quark,

$$\frac{Z_{X \neq V}}{Z_V}(a, m_\pi) = \frac{Z_X}{Z_V}(a, 0) \times (1 + c_1^X m_\pi^2), \quad (12)$$

where we assume the light quark dependence at different lattice spacing to be similar which is supported by the $\chi^2/\text{d.o.f} \sim 1$ we obtained. For Z_V and Z_V^c which is much more precise due to the high precision pseudoscalar correlation functions, we also include the strange sea and finite volume effects in the fit,

$$Z_V(a, m_\pi, m_{\eta_s}, 1/L) = Z_V(a, 0, 0, 0) (1 + c_1 m_\pi^2 + c_2 m_{\eta_s}^2 + c_3 e^{-m_\pi L}), \quad (13)$$

and re-scale the uncertainty by $\sqrt{\chi^2/\text{d.o.f}}$. All the chiral-extrapolated renormalization constants are collected in Table II and the numbers on each ensemble without chiral

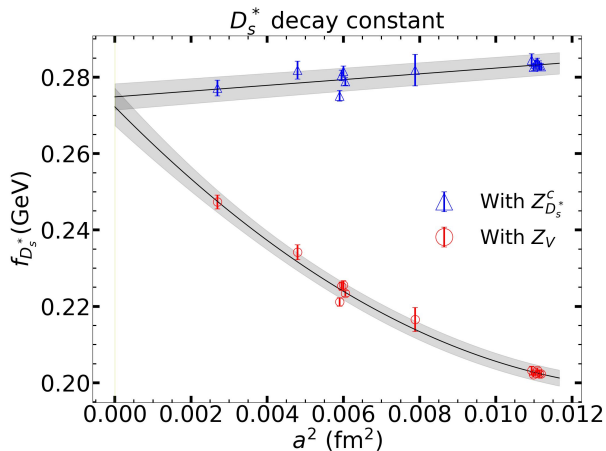


FIG. 7. Comparison of $f_{D_s^*}$ using heavy quark improved normalization constant $Z_V^{cl} \equiv \sqrt{Z_V Z_V^c}$ and original normalization constants Z_V at different lattice spacing and continuum. The continuum limits obtained for both cases are consistent with each other, but the discretization error for the former is smaller.

extrapolation can be found in Table IV in the appendix. It can be observed that Z_V^c is a factor of 2 larger than Z_V at the coarsest lattice spacing, while becomes much closer at the finest one.

III. RESULTS

Similar to our previous work [9], we perform bootstrap re-samplings on each ensemble and conduct the correlated global fit based on these bootstrap samples. The lattice spacing and renormalization constants are also sampled for each bootstrap sample using a Gaussian distribution with their uncertainties as the width of the distribution. Thus our results presented in this section have included the systematic uncertainties from the lattice spacing determination and non-perturbative renormalization.

For the dimensional quantity X in this section, we employ the following joint fit, which describes the results well with $\chi^2/\text{d.o.f} \sim 1$,

$$X(m_\pi, m_{\eta_s}, a) = X(m_\pi^{\text{phys}}, m_{\eta_s}^{\text{phys}}, 0) + d_1^X (m_\pi^2 - (m_\pi^{\text{phys}})^2) + d_2^X (m_{\eta_s}^2 - (m_{\eta_s}^{\text{phys}})^2) + d_3^X a^2 + d_4^X a^4, \quad (14)$$

where $m_\pi^{\text{phys}} = 134.98$ MeV is the physical π^0 mass, and the squares of the pion and η_s masses are used to account for the dependence on the light quark mass and strange sea quark masses (as the strange valence quark mass has been interpolated to its physical value), respectively. The $a^2 + a^4$ corrections are also introduced to describe the discretization error, and we will see that

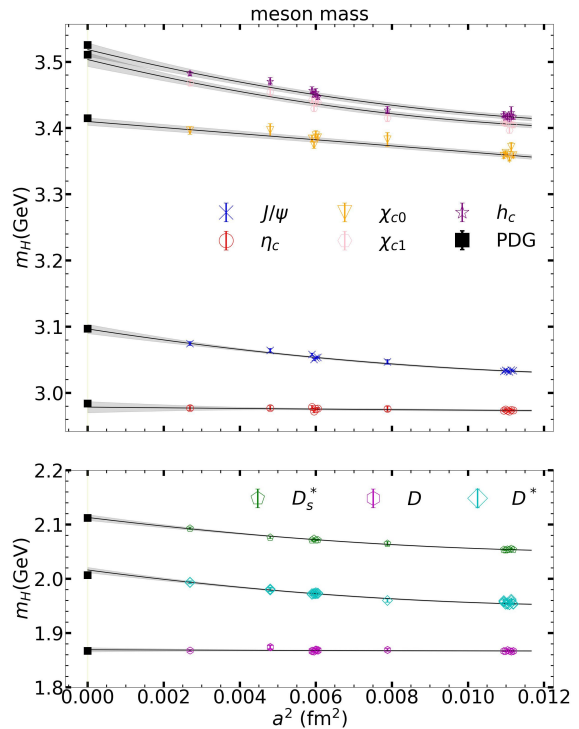


FIG. 8. The lattice spacing dependence of the charmonium masses (upper panel), and pseudoscalar and vector open-charm meson masses (lower panel) except the m_{D_s} which is used to tune the charm quark mass. The experimental values are shown as black stars for comparison. The light and strange sea quark masses have been corrected to their physical values using the parameters determined from the joint fit.

the a^4 term is essential for certain cases, especially the charm quark mass under $\overline{\text{MS}}$ 2 GeV. The aa_s term is not taken into account as it should be mainly removed by the non-perturbative renormalization, and our previous study [9] suggests that a^2 extrapolation works well for light flavor physics. Based on the joint fit, one can further eliminate the impact from the unphysical light and strange quark masses by subtracting the $d_{1,2}^X$ terms from $X(m_\pi, m_{\eta_s}, a)$ and obtain $X(m_\pi^{\text{phys}}, m_{\eta_s}^{\text{phys}}, a)$ with physical light and strange quark masses but at a finite lattice spacing.

While our systematic uncertainties stemming from discretization errors and unphysical light and strange quark masses have been mitigated through the joint fit outlined in Eq. (14), there remains a systematic uncertainty arising from the fit ansatz (such as the cross term $a^2 m_\pi^2$ and/or higher-order term m_π^4). Thus we can also fit the data using the following modified parameterization,

$$X(m_\pi, m_{\eta_s}, a) = [X'(m_\pi^{\text{phys}}, m_{\eta_s}^{\text{phys}}, 0) + d_1'^X (m_\pi^2 - (m_\pi^{\text{phys}})^2) + d_2'^X (m_{\eta_s}^2 - (m_{\eta_s}^{\text{phys}})^2)] (1 + d_3'^X a^2 + d_4'^X a^4), \quad (15)$$

TABLE II. Z_V, Z_V^c and ratios of different renormalization constants at different lattice spacing

a (fm)	Z_V	Z_V^c	Z_A/Z_V	Z_S/Z_V	Z_P/Z_V	Z_T/Z_V
0.10530(18)	0.8001(05)	1.5744(17)	1.0728(04)	1.2013(31)	0.9239(48)	1.0816(06)
0.08877(30)	0.8203(07)	1.4042(20)	1.0561(12)	1.0948(75)	0.8640(99)	1.0958(18)
0.07750(18)	0.8365(05)	1.3071(13)	1.0537(05)	1.0487(30)	0.8428(39)	1.1021(07)
0.06826(27)	0.8478(06)	1.2392(14)	1.0423(06)	1.0052(74)	0.8149(47)	1.1101(13)
0.05187(26)	0.8703(06)	1.1321(15)	1.0353(08)	0.9162(95)	0.7842(62)	1.1238(14)

and estimate the systematic uncertainty from the fit ansatz. Such an estimate turns out to be much smaller than the other uncertainties and can be refined when ensembles with a wider range of lattice spacings and quark masses become available.

Fig 8 shows the lattice spacing dependence of m_D^{QCD} , $m_{D^*}^{\text{QCD}}$ and $m_{D_s^*}^{\text{QCD}}$, with the impact from the unphysical light and strange quark masses subtracted using the fit ansatz defined in Eq. (14). The good agreement of the fit curve as a function of a^2 with our data points (with unphysical light and strange quark mass effects subtracted) also justifies our fit ansatz. Our predictions of m_D based on the joint fit are

$$\begin{aligned}
m_D^{\text{QCD}} &= 1869.2(4.0) \text{ MeV}, \\
m_{D^\pm}^{\text{QCD}} - m_{D^0}^{\text{QCD}} &= d_1^D \frac{(m_\pi^{\text{phys}})^2}{m_l} (m_d - m_u) + \mathcal{O}\left(\frac{m_l^2}{\Lambda_\chi}\right) \\
&= 2.87(26) \text{ MeV}, \tag{16}
\end{aligned}$$

where we use the leading order chiral perturbative theory approximation and $\frac{(m_\pi^{\text{phys}})^2}{m_l} (m_d - m_u) = 0.0116(8) \text{ GeV}^2$ based on our previous work [9]. They perfectly agree with the experimental values with the QED correction from literature (provided in Ref. [6] and updated in Ref. [13]) subtracted, $m_D^{\text{QCD}} = 1866.3(0.7) \text{ MeV}$ and $m_{D^\pm}^{\text{QCD}} - m_{D^0}^{\text{QCD}} = 2.5(0.5) \text{ MeV}$.

At the same time, our prediction of the D^* mass (light blue) and the D_s^* mass (green) are consistent with the experimental value. The unknown QED effect of the vector meson masses can be significant if the statistics uncertainty can be further suppressed.

For the charmonium mass, we can see from Fig. 8 that the central values of both $m_{J/\psi}$ and m_{η_c} are a few MeV lower than the experimental values, respectively. The disconnected diagram and QED effects would not be important at the present precision.

At the same time, our prediction of the hyperfine splitting is

$$\Delta_{\text{HFS}, \bar{c}c}^{\text{QCD, conn}} = m_{J/\psi}^{\text{QCD, conn}} - m_{\eta_c}^{\text{QCD, conn}} = 118.0(2.8) \text{ MeV}, \tag{17}$$

and consistent with the previous HPQCD study [21] using staggered fermions, 118.6(1.1) MeV. Such a value is slightly larger than the experimental value 113.0(5) [19]. The difference can be attributed mostly to the quark annihilation effect (The correction from the QED effect is around 1 MeV [21]). Direct calculations using anisotropic

$N_f=2$ charm quark sea ensemble at $a_t = 0.0205 \text{ fm}$ with $a_s/a_t = 5$ indicate that the inclusion of charm quark annihilation diagram almost does not change the J/ψ mass, but pushes the η_c mass up by approximately 3-4 MeV [22, 23], regardless of whether the mixing with the pseudo-scalar glueball is considered.

Given the approximation

$$m_{h_c} = \frac{1}{9}(m_{\chi_{c0}} + 3m_{\chi_{c1}} + 5m_{\chi_{c2}}) \tag{18}$$

which has been verified by the experiment at 0.1 MeV level and can be explained by the short range feature of the spin-spin interaction in the context of potential models [24, 25], we skipped the calculation of the χ_{c2} mass which requires additional complication in the interpolating field, and extract the following three splittings based on $m_{\chi_{c0}, \chi_{c1}, h_c}$ we obtained,

$$\begin{aligned}
\Delta_{1P-1S, \bar{c}c}^{\text{QCD, conn}} &= m_{h_c} - \frac{1}{4}(3m_{J/\psi} + m_{\eta_c}) \\
&= 451(11) \text{ MeV}, \\
\Delta_{1P_{\text{spin-orbit}}, \bar{c}c}^{\text{QCD, conn}} &= \frac{1}{3}(3m_{h_c} - m_{\chi_{c0}} - 2m_{\chi_{c1}}) \\
&= 46.3(9.5) \text{ MeV}, \\
\Delta_{1P_{\text{tensor}}, \bar{c}c}^{\text{QCD, conn}} &= \frac{1}{5}(-m_{h_c} - m_{\chi_{c0}} + 2m_{\chi_{c1}}) \\
&= 15.7(3.8) \text{ MeV}. \tag{19}
\end{aligned}$$

All of three splittings agree with the experimental value and previous LQCD calculation using the HISQ fermion [26] well within the uncertainty.

From Fig. 8, we can also see that the pseudo-scalar meson masses have much smaller lattice spacing dependence than the vector meson masses, since our valence strange and charm quark masses are also determined using the pseudo scalar masses. The lattice spacing dependence of the vector meson masses also suggests that the hyperfine splitting Δ_{HFS} will exhibit a significant variation, which is crucial for ensuring that the continuum extrapolated values of Δ_{HFS} closely match the physical values.

Using the charm quark improved normalization, the decay constants of the pseudo-scalar and vector open-charm mesons and charmonium at different lattice spacings are illustrated in Fig. 9. The decay constants of the open-charm mesons exhibit negligible lattice spacing dependence and are consistent with the previous HPQCD results using the HISQ action within a 1-2% uncertainty. For the values of $f_{J/\psi}$ and f_{η_c} , after using the charm quark

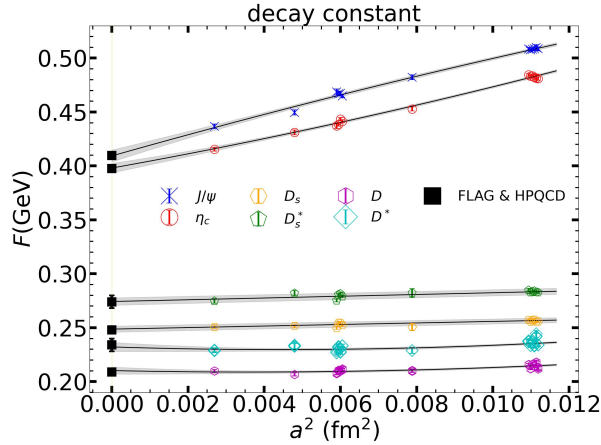


FIG. 9. Similar to Fig. 8 but for the decay constants.

improved normalization, the lattice spacing dependence is weakened and our final predictions are consistent with that from HPQCD.

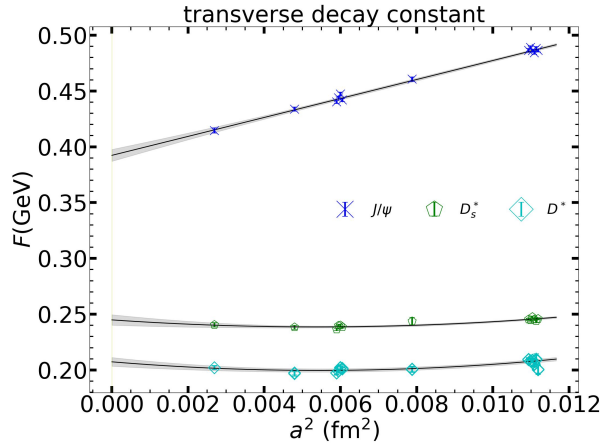


FIG. 10. Similar to Fig. 8 but for the transverse decay constants.

In addition, we show the lattice spacing dependence of transverse decay constant of the charmed vector mesons in Fig. 10 and also those of the P-wave charmonium in Fig. 11.

Using a similar approach as outlined in Ref. [9] for the light and strange quarks, the renormalized charm quark mass at $\overline{\text{MS}}$ 2 GeV with $N_f = 3$ matching and running is determined for each ensemble. One can further obtain the charm quark mass in the continuum and also physical light and strange quark mass by using the joint fit the data on different ensembles. After correcting for small effects arising from the unphysical light and strange quark masses, the renormalized charm quark masses on all the ensembles with different lattice spacings are depicted in Fig. 12. It is evident that at the largest lattice spacing,

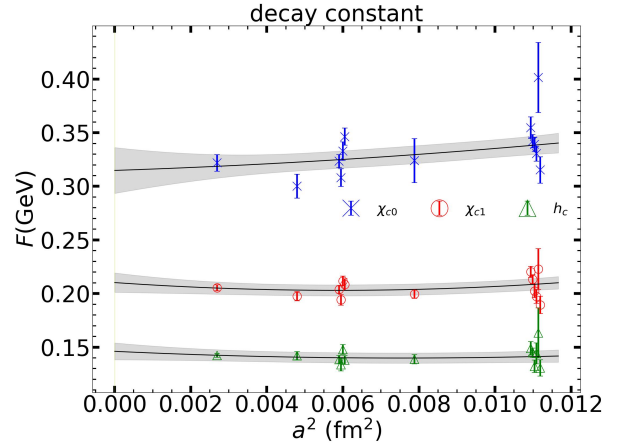


FIG. 11. Similar to Fig. 8 but for the P-wave charmonium decay constants.

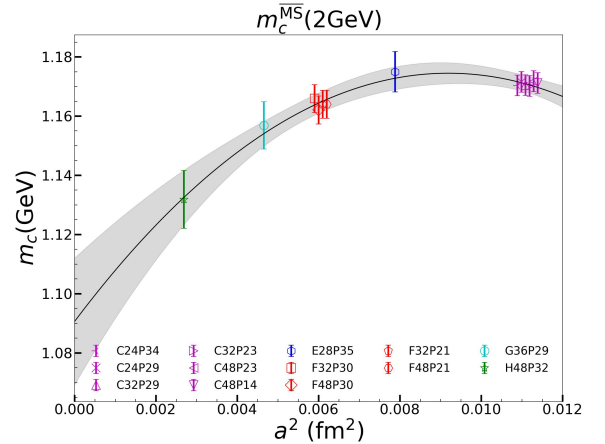


FIG. 12. The lattice spacing dependence of the physical charm quark mass under $\overline{\text{MS}}$ scheme 2 GeV on all the ensembles at different lattice spacings. The light and strange sea quark masses have been adjusted to their physical values based on the parameters derived from the joint fit.

m_c deviates by $\sim 10\%$ from its continuum extrapolated value, based on a $a^2 + a^4$ extrapolation. Converting the charm quark mass to $m_c(m_c)$ using perturbative running yields a value of $1.289(17)$ GeV, with systematic uncertainties from lattice spacing determination and renormalization.

Eventually we just collect our predictions in Table III for comparison. Using the results of f_D and f_{D_s} , one can extract the CKM matrix elements $|V_{cd}|$ and $|V_{cs}|$, respectively. Taking into account the experimental constraints on the products of decay constants and CKM matrix elements [19], as given below

$$\begin{aligned} f_{D^+} |V_{cd}| &= 45.8(1.1)\text{MeV} \\ f_{D_s^+} |V_{cs}| &= 243.5(2.7)\text{MeV} \end{aligned} \quad (20)$$

TABLE III. Charm quark mass under the $\overline{\text{MS}}$ scheme, charmed meson masses, and also related decay constants. The so-call “Pure QCD” values corresponds to the values from literatures without annihilation diagram or QED correction. All the values are in unit of GeV.

	$m_c(m_c)$		m_D	m_{D^*}	$m_{D_s^*}$	
This work	1.289(17)(01)		1.8692(40)(01)	2.0162(49)(10)	2.1130(54)(02)	
FLAG/Exp.	1.276(05)		1.8672(2)	2.00856(5)	2.1122(04)	
	m_{η_c}	$m_{J/\psi}$	$m_{\chi_{c0}}$	$m_{\chi_{c1}}$	m_{h_c}	
This work	2.9786(85)(01)	3.0967(69)(01)	3.4099(57)(01)	3.503(10)(01)	3.519(10)(01)	
Exp.	2.9841(4)	3.09690(1)	3.41471(30)	3.51067(5)	3.52537(14)	
	$\Delta_{\text{HFS},\bar{c}l}$	$\Delta_{\text{HFS},\bar{c}s}$	$\Delta_{\text{HFS},\bar{c}c}$	$\Delta_{1P_{\text{spin-orbit}},\bar{c}c}$	$\Delta_{1P_{\text{tensor}},\bar{c}c}$	$\Delta_{1P-1S,\bar{c}c}$
This work	0.1470(47)(10)	0.1463(54)(02)	0.1180(28)(02)	0.0463(95)(03)	0.0157(38)(01)	0.451(11)(01)
Literature			0.1186(11) [20]	0.0433(66) $^{+10}_{-0}$ [26]	0.0150(23) $^{+3}_{-0}$ [26]	0.469(11) $^{+10}_{-0}$ [26]
Exp.	0.1413(01)	0.1438(04)	0.1128(04)	0.04669(18)	0.016252(69)	0.45659(11)
	f_D	f_{D^*}	$f_{D^*}^T$	f_{D_s}	$f_{D_s^*}$	$f_{D_s^*}^T$
This work	0.2102(33)(03)	0.2321(43)(01)	0.2073(39)(08)	0.2487(28)(02)	0.2743(34)(01)	0.2449(47)(01)
Literature	0.2090(24) [5]	0.234(6) [27]	0.192(14) [28]	0.2480(16) [5]	0.274(6) [29]	0.252(10) [28]
	f_{η_c}	$f_{J/\psi}$	$f_{J/\psi}^T$	$f_{\chi_{c0}}$	$f_{\chi_{c1}}$	f_{h_c}
This work	0.3981(44)(14)	0.4059(51)(25)	0.3923(53)(18)	0.314(23)(01)	0.2105(91)(03)	0.1464(80)(03)
Literature	0.3975(10) [20]	0.4096(16) [20]	0.3911(56) [28]			

and combining with our results summarized in Table. III, we finally obtain

$$|V_{cd}| = 0.2179(33)(52), \quad |V_{cs}| = 0.979(11)(11), \quad (21)$$

where the first errors come from the lattice results and the second result from the uncertainties from the experiments in Eq. (20). The above results are consistent with those quoted by the PDG, but with slight larger errors. Using the present PDG value of $|V_{cb}| = 0.041(1)$ [19] which is negligible comparing to the uncertainties of $|V_{cd(s)}|$, we predict,

$$|V_{cd}|^2 + |V_{cs}|^2 + |V_{cb}|^2 = 1.008(23)(23), \quad (22)$$

and verify the unity of the unitarity of the CKM matrix elements involving the charm quark.

Our predictions of the quantities f_{D^*} and $f_{D_s^*}$ are by far the most precise. Comparing with the previous results [27–29], our calculation provides much better control on the systematic uncertainties on the unphysical sea quark masses and discretization error, and then also by far the most accurate. Therefore, we can provide insight into the experimental search for the purely leptonic decay of D^* and D_s^* particles. Most recently, the BESIII collaboration has reported the first experimental measurements on the purely leptonic decays $D^* \rightarrow l\nu_l$ [30] and $D_s^* \rightarrow l\nu_l$ [31] with $l = e, \mu$. No significant signal is observed for the channel $D^* \rightarrow l\nu_l$, and only upper limits are set as $\text{Br}(D^* \rightarrow e\nu_e) < 1.1 \times 10^{-5}$ and $\text{Br}(D^* \rightarrow \mu\nu_\mu) < 4.3 \times 10^{-6}$. For $D_s^* \rightarrow l\nu_l$, the BESIII gives the branching fraction of this decay as $(2.1^{+1.2}_{-0.9\text{stat.}} \pm 0.2\text{syst.}) \times 10^{-5}$. Theoretically, the decay widths of these pure leptonic decays can be parameterized by the f_{D^*} and $f_{D_s^*}$ via the following way

$$\Gamma = \frac{G_F^2}{12\pi} |V_{cd(s)}|^2 f_V^2 m_V^3 \left(1 - \frac{m_l^2}{m_V^2}\right)^2 \left(1 + \frac{m_l^2}{2m_V^2}\right) \quad (23)$$

where the symbol V denotes the vector mesons D^* and D_s^* , respectively, and m_l is the mass of lepton $l = e, \mu$. Using the most precise CKM matrix elements $V_{cd} = 0.221(4)$, $V_{cs} = 0.975(7)$ [5] determined from the lattice calculation of the $D_{(s)}$ meson semileptonic decays and our predictions of f_{D^*/D_s^*} , we then find the decay width,

$$\begin{aligned} \Gamma(D^* \rightarrow l\nu_l)_{l=e,\mu} &= 3.54(16) \times 10^{-7} \text{ keV}, \\ \Gamma(D_s^* \rightarrow l\nu_l)_{l=e,\mu} &= 2.41(09) \times 10^{-6} \text{ keV}, \end{aligned} \quad (24)$$

The branching fractions of them can then be determined by combining with the total decay width $\Gamma_{\text{total}}(D^*) = 83.4(1.8) \text{ keV}$ [19] and $\Gamma_{\text{total}}(D_s^*) = 0.0587(54) \text{ keV}$ [32]. The results are given as $\text{Br}(D^* \rightarrow l\nu_l) = 4.24(09)(19) \times 10^{-9}$ and $\text{Br}(D_s^* \rightarrow l\nu_l) = 4.11(38)(15) \times 10^{-5}$.

IV. SUMMARY

In this work, we determine the charm quark mass using the D_s meson mass and convert it to the $\overline{\text{MS}}$ scheme, and then predict the charmed meson masses and their decay constants. The results are summarized in Table III. The values from PDG [19], FLAG [5] and HPQCD [20, 29] are also listed there for comparison. All our predictions of the charmed meson masses are consistent with the experimental value at 0.3% level uncertainty. We also verified the unitarity of the CKM matrix elements involving the charm quark at 3% level, updated the constraints on the leptonic decay width of $D_{(s)}^*$, and provide the decay constants of the P-wave charmonium decay constants in the continuum with physical quark masses for the first time (?).

In the above predictions, we used the interpolated strange quark mass, which corresponds to the “physical” η_s mass [12]. This mass may differ by 10-15% from the unitary strange quark mass on certain ensembles, and its

use can effectively suppress the impact of the unphysical strange quark mass on those ensembles by an order of magnitude in the D_s^* mass.

Comparing to the overlap fermion where $Z_V = Z_A$ only depends on $m_{\text{PS}}^2 a^2$ with a tiny coefficient ~ 0.02 [33, 34], the clover fermion we used here has a much stronger $m_{\text{PS}}^2 a^2$ dependence with a coefficient ~ 0.5 . It makes the continuum extrapolation using the heavy quark improved Z_V^c normalization has much smaller discretization error for the charmed meson matrix elements comparing to that using the mass-independent one. The values of the renormalization constants are collect in Table II.

In summary, we would expect the previous [32, 35–41] and ongoing studies using the CLQCD ensembles [9] for the charm physics can reach higher accuracy with the interpolated charm and strange quark masses and also the heavy quark improved normalization scheme presented in this work. More specifically, hopefully the systematic uncertainties coming from the unphysical light and strange quark masses and finite lattice spacing can be controlled using the CLQCD ensembles, in the spectrum, form factors, semi-leptonic decay, and behaviors at the finite temperature and magnetic field of light and charmed meson and baryon.

ACKNOWLEDGEMENT

We thank the CLQCD collaborations for providing us their gauge configurations with dynamical fermions [9], which are generated on HPC Cluster of ITP-CAS, the Southern Nuclear Science Computing Center(SNSC) and the Siyuan-1 cluster supported by the Center for High Performance Computing at Shanghai Jiao Tong University. The calculations were performed using the Chroma software suite [42] with QUDA [43–45] through HIP programming model [46]. We also thank Christine Davies for helpful discussion. The numerical calculation were carried out on the ORISE Supercomputer, HPC Cluster of ITP-CAS and Advanced Computing East China Sub-center. This work is supported in part by NSFC grants No. 12293060, 12293062, 12293061, 12293063, 12293064, 12293065, 12047503, 12175279 and 11935017, the science and education integration young faculty project of University of Chinese Academy of Sciences, the Strategic Priority Research Program of Chinese Academy of Sciences, Grant No. XDB34030303, XDB34030301 and YSBR-101, and also a NSFC-DFG joint grant under Grant No. 12061131006 and SCHA 458/22.

-
- [1] M. Ablikim *et al.* (BESIII), *Phys. Rev. Lett.* **110**, 252001 (2013), [arXiv:1303.5949 \[hep-ex\]](#).
- [2] Z. Q. Liu *et al.* (Belle), *Phys. Rev. Lett.* **110**, 252002 (2013), [Erratum: *Phys.Rev.Lett.* 111, 019901 (2013)], [arXiv:1304.0121 \[hep-ex\]](#).
- [3] J.-J. Wu, R. Molina, E. Oset, and B. S. Zou, *Phys. Rev. Lett.* **105**, 232001 (2010), [arXiv:1007.0573 \[nucl-th\]](#).
- [4] R. Aaij *et al.* (LHCb), *Phys. Rev. Lett.* **115**, 072001 (2015), [arXiv:1507.03414 \[hep-ex\]](#).
- [5] Y. Aoki *et al.* (Flavour Lattice Averaging Group (FLAG)), *Eur. Phys. J. C* **82**, 869 (2022), [arXiv:2111.09849 \[hep-lat\]](#).
- [6] D. Giusti, V. Lubicz, C. Tarantino, G. Martinelli, F. Sanfilippo, S. Simula, and N. Tantalo, *Phys. Rev. D* **95**, 114504 (2017), [arXiv:1704.06561 \[hep-lat\]](#).
- [7] X. Feng and L. Jin, *Phys. Rev. D* **100**, 094509 (2019), [arXiv:1812.09817 \[hep-lat\]](#).
- [8] J. Heitger, F. Joswig, and S. Kuberski (ALPHA), *JHEP* **05**, 288 (2021), [arXiv:2101.02694 \[hep-lat\]](#).
- [9] Z.-C. Hu *et al.* (CLQCD), *Phys. Rev. D* **109**, 054507 (2024), [arXiv:2310.00814 \[hep-lat\]](#).
- [10] M. Lüscher, *JHEP* **08**, 071 (2010), [Erratum: *JHEP* 03, 092 (2014)], [arXiv:1006.4518 \[hep-lat\]](#).
- [11] S. Borsanyi *et al.* (BMW), *JHEP* **09**, 010 (2012), [arXiv:1203.4469 \[hep-lat\]](#).
- [12] S. Borsanyi *et al.*, *Nature* **593**, 51 (2021), [arXiv:2002.12347 \[hep-lat\]](#).
- [13] M. Di Carlo, D. Giusti, V. Lubicz, G. Martinelli, C. T. Sachrajda, F. Sanfilippo, S. Simula, and N. Tantalo, *Phys. Rev. D* **100**, 034514 (2019), [arXiv:1904.08731 \[hep-lat\]](#).
- [14] J. Gasser, A. Rusetsky, and I. Scimemi, *Eur. Phys. J. C* **32**, 97 (2003), [arXiv:hep-ph/0305260](#).
- [15] T. Ishikawa *et al.* (JLQCD), *Phys. Rev. D* **78**, 011502 (2008), [arXiv:0704.1937 \[hep-lat\]](#).
- [16] Z. Liu, Y. Chen, S.-J. Dong, M. Glatzmaier, M. Gong, A. Li, K.-F. Liu, Y.-B. Yang, and J.-B. Zhang (chiQCD), *Phys. Rev. D* **90**, 034505 (2014), [arXiv:1312.7628 \[hep-lat\]](#).
- [17] G. Martinelli, C. Pittori, C. T. Sachrajda, M. Testa, and A. Vladikas, *Nucl. Phys.* **B445**, 81 (1995), [arXiv:hep-lat/9411010 \[hep-lat\]](#).
- [18] K. Zhang, Y.-Y. Li, Y.-K. Huo, A. Schäfer, P. Sun, and Y.-B. Yang (χ QCD), *Phys. Rev. D* **104**, 074501 (2021), [arXiv:2012.05448 \[hep-lat\]](#).
- [19] R. L. Workman *et al.* (Particle Data Group), *PTEP* **2022**, 083C01 (2022).
- [20] D. Hatton, C. T. H. Davies, B. Galloway, J. Koponen, G. P. Lepage, and A. T. Lytle (HPQCD), *Phys. Rev. D* **102**, 054511 (2020), [arXiv:2005.01845 \[hep-lat\]](#).
- [21] D. Hatton, C. T. H. Davies, B. Galloway, J. Koponen, G. P. Lepage, and A. T. Lytle (HPQCD), *Phys. Rev. D* **102**, 054511 (2020), [arXiv:2005.01845 \[hep-lat\]](#).
- [22] R. Zhang, W. Sun, F. Chen, M. G. Ying Chen and, X. Jiang, and Z. Liu, *Chin. Phys. C* **46**, 043102 (2022), [arXiv:2110.01755 \[hep-lat\]](#).
- [23] R. Zhang, W. Sun, Y. Chen, M. Gong, L.-C. Gui, and Z. Liu, *Phys. Lett. B* **827**, 136960 (2022), [arXiv:2107.12749 \[hep-lat\]](#).
- [24] W. Kwong, J. L. Rosner, and C. Quigg, *Ann. Rev. Nucl. Part. Sci.* **37**, 325 (1987).
- [25] W. Lucha, F. F. Schoberl, and D. Gromes, *Phys. Rept.* **200**, 127 (1991).
- [26] T. Burch, C. DeTar, M. Di Pierro, A. X. El-Khadra, E. D. Freeland, S. Gottlieb, A. S. Kronfeld, L. Levkova, P. B. Mackenzie, and J. N. Simone, *Phys. Rev. D* **81**, 034508

- (2010), [arXiv:0912.2701 \[hep-lat\]](#).
- [27] Y. Chen, C. Wei-Feng, M. Gong, Z. Liu, and Y. Ma, *Chin. Phys. C* **45**, 023109 (2021), [arXiv:2008.05208 \[hep-lat\]](#).
- [28] D. Li, Y. Chen, M. Gong, K.-F. Liu, Z. Liu, and T. Wang, (2024), [arXiv:2407.03697 \[hep-lat\]](#).
- [29] G. C. Donald, C. T. H. Davies, J. Koponen, and G. P. Lepage (HPQCD), *Phys. Rev. Lett.* **112**, 212002 (2014), [arXiv:1312.5264 \[hep-lat\]](#).
- [30] M. Ablikim *et al.* (BESIII), *Phys. Rev. D* **110**, 012003 (2024), [arXiv:2405.09066 \[hep-ex\]](#).
- [31] M. Ablikim *et al.* (BESIII), *Phys. Rev. Lett.* **131**, 141802 (2023), [arXiv:2304.12159 \[hep-ex\]](#).
- [32] Y. Meng, J.-L. Dang, C. Liu, Z. Liu, T. Shen, H. Yan, and K.-L. Zhang, *Phys. Rev. D* **109**, 074511 (2024), [arXiv:2401.13475 \[hep-lat\]](#).
- [33] G. Wang, J. Liang, T. Draper, K.-F. Liu, and Y.-B. Yang (chiQCD), *Phys. Rev. D* **104**, 074502 (2021), [arXiv:2006.05431 \[hep-ph\]](#).
- [34] F. He, Y.-J. Bi, T. Draper, K.-F. Liu, Z. Liu, and Y.-B. Yang (χ QCD), *Phys. Rev. D* **106**, 114506 (2022), [arXiv:2204.09246 \[hep-lat\]](#).
- [35] Q.-A. Zhang *et al.*, *Chin. Phys. C* **46**, 011002 (2022), [arXiv:2103.07064 \[hep-lat\]](#).
- [36] H. Xing, J. Liang, L. Liu, P. Sun, and Y.-B. Yang, (2022), [arXiv:2210.08555 \[hep-lat\]](#).
- [37] H. Liu, L. Liu, P. Sun, W. Sun, J.-X. Tan, W. Wang, Y.-B. Yang, and Q.-A. Zhang, *Phys. Lett. B* **841**, 137941 (2023), [arXiv:2303.17865 \[hep-lat\]](#).
- [38] H. Liu, W. Wang, and Q.-A. Zhang, *Phys. Rev. D* **109**, 036037 (2024), [arXiv:2309.05432 \[hep-ph\]](#).
- [39] H. Liu, J. He, L. Liu, P. Sun, W. Wang, Y.-B. Yang, and Q.-A. Zhang, *Sci. China Phys. Mech. Astron.* **67**, 211011 (2024), [arXiv:2207.00183 \[hep-lat\]](#).
- [40] X.-Y. Han, J. Hua, X. Ji, C.-D. Lü, W. Wang, J. Xu, Q.-A. Zhang, and S. Zhao, (2024), [arXiv:2403.17492 \[hep-ph\]](#).
- [41] H. Yan, C. Liu, L. Liu, Y. Meng, and H. Xing, (2024), [arXiv:2404.13479 \[hep-lat\]](#).
- [42] R. G. Edwards and B. Joo (SciDAC, LHPC, UKQCD), *Lattice field theory. Proceedings, 22nd International Symposium, Lattice 2004, Batavia, USA, June 21-26, 2004*, *Nucl. Phys. Proc. Suppl.* **140**, 832 (2005), [832(2004)], [arXiv:hep-lat/0409003 \[hep-lat\]](#).
- [43] M. A. Clark, R. Babich, K. Barros, R. C. Brower, and C. Rebbi, *Comput. Phys. Commun.* **181**, 1517 (2010), [arXiv:0911.3191 \[hep-lat\]](#).
- [44] R. Babich, M. A. Clark, B. Joo, G. Shi, R. C. Brower, and S. Gottlieb, in *SC11 International Conference for High Performance Computing, Networking, Storage and Analysis Seattle, Washington, November 12-18, 2011* (2011) [arXiv:1109.2935 \[hep-lat\]](#).
- [45] M. A. Clark, B. Jo, A. Strelchenko, M. Cheng, A. Gambhir, and R. Brower, (2016), [arXiv:1612.07873 \[hep-lat\]](#).
- [46] Y.-J. Bi, Y. Xiao, M. Gong, W.-Y. Guo, P. Sun, S. Xu, and Y.-B. Yang, *Proceedings, 37th International Symposium on Lattice Field Theory (Lattice 2019): Wuhan, China, June 16-22 2019*, *PoS LATTICE2019*, 286 (2020), [arXiv:2001.05706 \[hep-lat\]](#).

APPENDIX

A. Autocorrelation

For the lattice configurations generated by the hybrid Monte Carlo, the autocorrelation between the trajectories is unavoidable. The independent configuration can only be obtained per each $\mathcal{O}(10)$ trajectories. To quantitatively evaluate the impact of autocorrelation, we employ a detailed statistical analysis focused on the variance of binned means:

1. **Overall Mean:** The overall mean, \bar{O} , of a measurement is computed as:

$$\bar{O} = \frac{1}{N} \sum_{i=1}^N O_i$$

where O_i denotes individual measurements within one trajectory.

2. **Binned Means:** For bin sizes varying from 1 to n_{\max} , the mean of observations within each bin is calculated as:

$$\bar{O}_{n,k} = \frac{1}{n} \sum_{i=(k-1)n+1}^{kn} O_i, \quad k = 1, 2, \dots, \left\lfloor \frac{N}{n} \right\rfloor$$

where k indexes the bins.

3. **Variance of Binned Means:** The variance of these binned means from the overall mean is given by:

$$\sigma_n^2(O) = \frac{1}{M-1} \sum_{k=1}^M (\bar{O}_{n,k} - \bar{O})^2$$

where $M = \left\lfloor \frac{N}{n} \right\rfloor$ is the number of complete bins.

4. Error in Variance Calculation: The standard error of the variance, providing a measure of its uncertainty, is computed as:

$$\text{SE}(\sigma_n^2) = \sqrt{\frac{1}{M(M-1)} \sum_{k=1}^M (s_{n,k}^2 - \sigma_n^2)^2}$$

where $s_{n,k}^2$ is the variance within each bin:

$$s_{n,k}^2(O) = \frac{1}{n-1} \sum_{i=(k-1)n+1}^{kn} (O_i - \bar{O}_{n,k})^2$$

We anticipate the variance of binned measurements will remain stable, assuming that the autocorrelation effects are sufficiently minimized. Here we compute both local and global quantities: the average plaquette value $\square = \langle \text{Tr } U_p \rangle / 3$, and the topological charge,

$$Q = \int d^4x q(x), \quad q(x) = \frac{g^2}{32\pi^2} \epsilon_{\mu\nu\rho\sigma} \text{Tr} [F^{\mu\nu}(x) F^{\rho\sigma}(x)]$$

along with the masses of pion and η_c . Figs. 13 and 14 show the normalized variance σ_n/σ_1 of these 4 quantities as functions of the bin size n within each ensemble.

B. Renormalization constants on each ensemble

The renormalization constants without the chiral extrapolation of the light sea quark masses on each ensemble are presented in Table IV. These values would be beneficial for readers interested in understanding the sea quark mass dependence of the renormalization constants.

TABLE IV. The renormalization constants on each ensemble.

a (fm)	Symbol	Z_V	Z_V^s (optional)	Z_V^c	Z_A/Z_V	Z_P/Z_V	Z_S/Z_V	Z_T/Z_V
0.10530(18)	C24P34	0.79676(32)	0.85034(10)	1.56730(20)	1.07677(72)	0.921(12)	1.205(05)	1.0856(20)
	C24P29	0.79814(23)	0.85184(06)	1.56970(18)	1.07244(70)	0.922(17)	1.194(06)	1.0825(10)
	C32P29	0.79810(13)	0.85167(04)	1.56859(15)	1.07648(63)	0.923(07)	1.199(08)	1.0826(10)
	C32P23	0.79957(13)	0.85350(04)	1.57246(12)	1.07375(40)	0.929(08)	1.197(06)	1.0818(10)
	C48P23	0.79954(05)	0.85339(02)	1.57062(08)	1.07317(70)	0.923(09)	1.208(10)	1.0819(10)
	C48P14	0.79957(06)	0.85359(02)	1.57057(08)	1.07320(68)	0.915(11)	1.204(04)	1.0831(10)
0.08877(30)	E28P35	0.81768(04)	0.85877(02)	1.39534(06)	1.06029(53)	0.862(06)	1.095(05)	1.0991(10)
0.07750(18)	F32P30	0.83548(12)	0.86900(03)	1.30240(08)	1.05549(54)	0.841(10)	1.042(09)	1.1036(10)
	F48P30	0.83511(04)	0.86880(02)	1.30109(06)	1.05687(66)	0.841(04)	1.053(09)	1.1052(10)
	F32P21	0.83579(09)	0.87031(03)	1.30517(08)	1.05416(50)	0.845(05)	1.042(06)	1.1008(10)
	F48P21	0.83567(05)	0.86880(02)	1.30456(04)	1.05434(88)	0.840(07)	1.051(04)	1.1033(10)
0.06826(27)	G36P29	0.84636(09)	0.87473(05)	1.23437(02)	1.04500(22)	0.814(03)	1.006(07)	1.1118(10)
0.05187(26)	H48P32	0.86855(04)	0.88780(01)	1.12690(10)	1.03802(28)	0.783(04)	0.916(09)	1.1260(10)

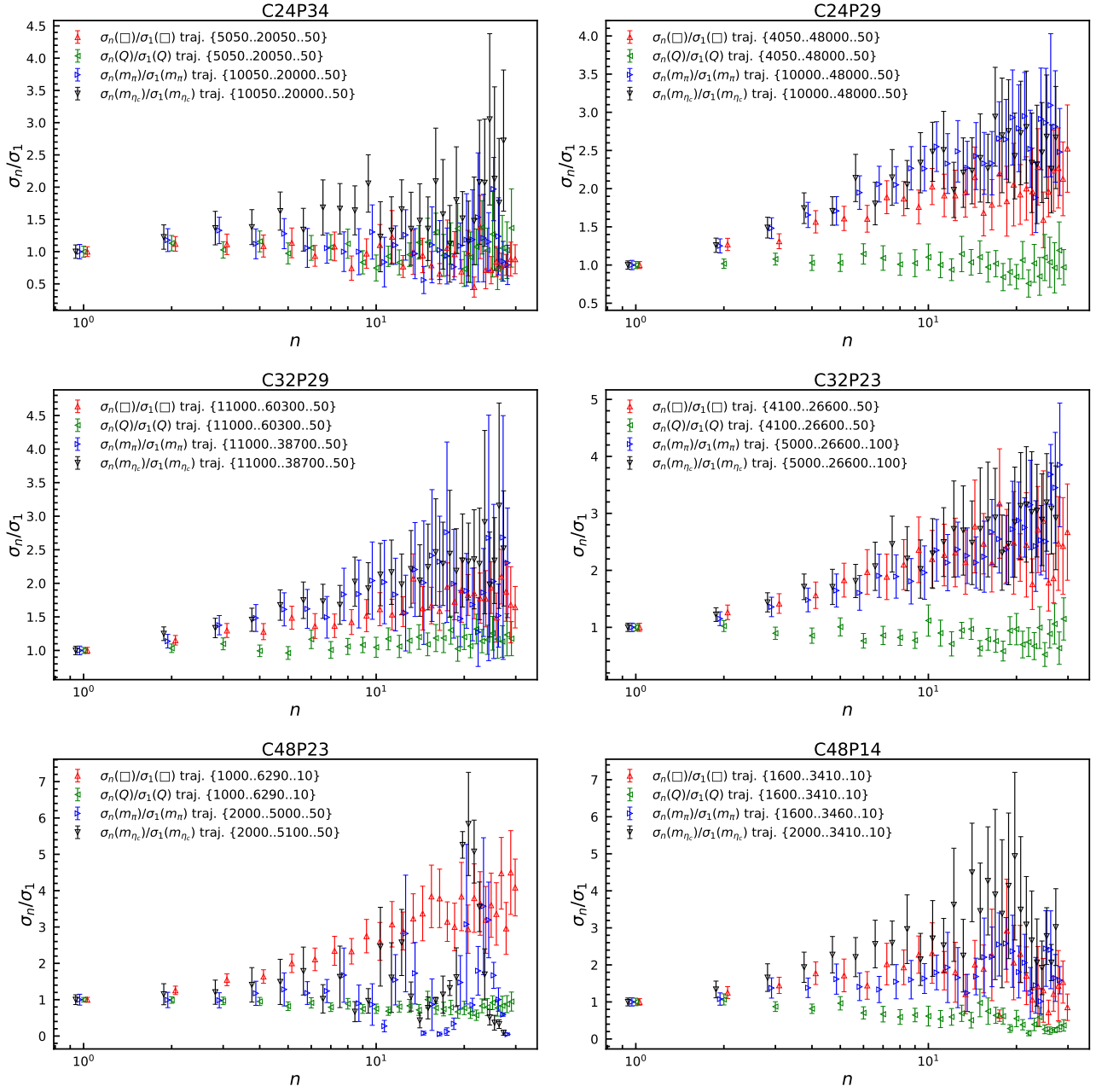


FIG. 13. Part 1 of the autocorrelation analysis. Each panel represents a different ensemble, illustrating the variance of four key measurements – plaquette value, topological charge, pion mass, and η_c mass, as functions of bin size n . The numbers $\{n_{\min}, n_{\max}, \delta n\}$ displayed in the label of each quantity correspond to the smallest and largest trajectory numbers, as well as the number of trajectories we skipped to obtain an independent configuration used in the figure.

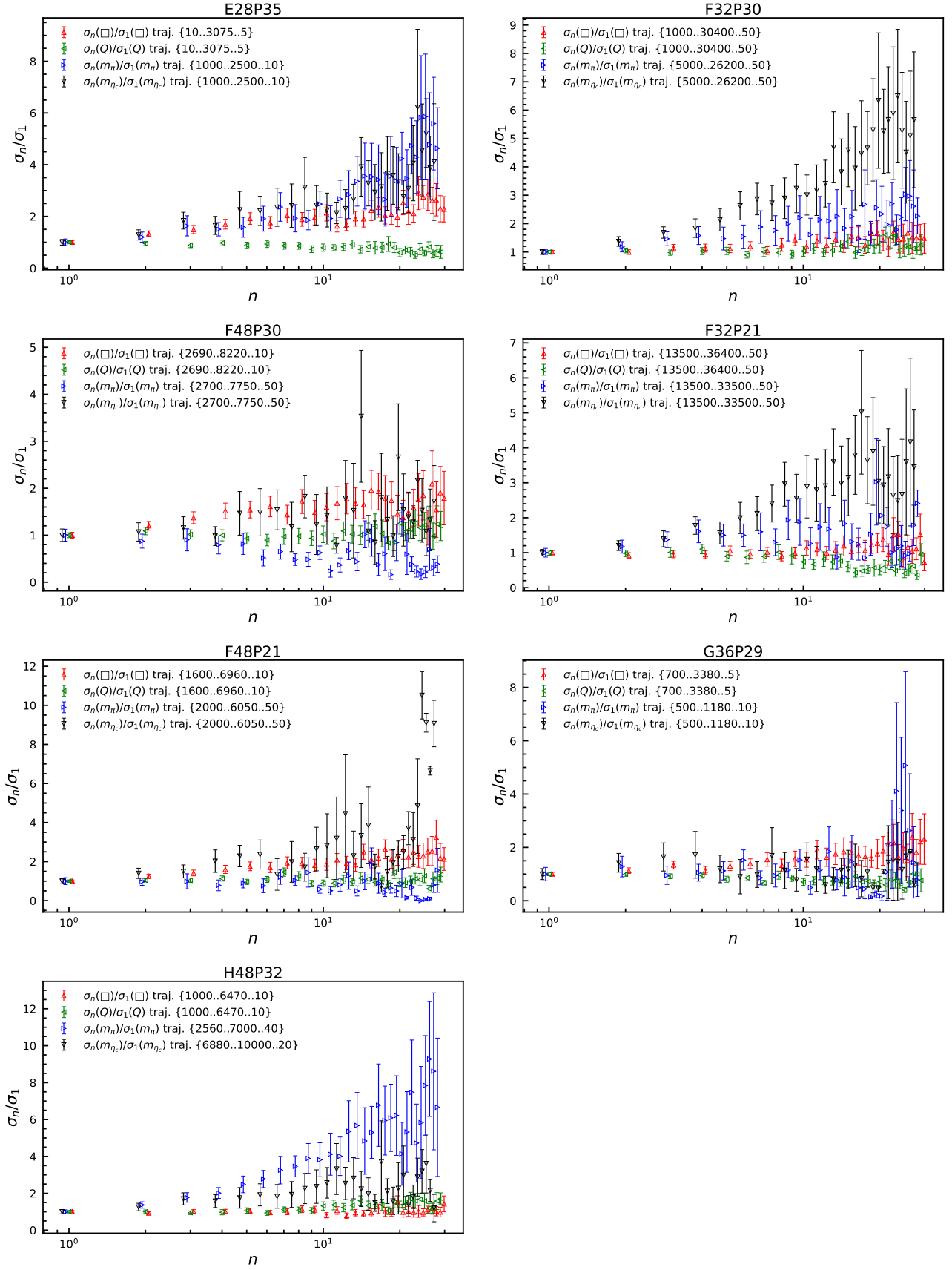


FIG. 14. Part 2 of the autocorrelation analysis.